UNIVERSIDADE DE SÃO PAULO
FACULDADE DE ODONTOLOGIA DE BAURU

LUCAS JOSÉ DE AZEVEDO SILVA

# Synthesis, characterization and mechanic evaluation of dense bovine hydroxyapatite ceramics with $TiO_2$ nanoparticles

# Síntese, caracterização e avaliação mecânica de cerâmica densa de hidroxiapatita bovina com nanopartículas de $TiO_2$

BAURU
2020

LUCAS JOSÉ DE AZEVEDO SILVA

# Synthesis, characterization and mechanic evaluation of dense bovine hydroxyapatite ceramics with $TiO_2$ nanoparticles

# Síntese, caracterização e avaliação mecânica de cerâmica densa de hidroxiapatita bovina com nanopartículas de $TiO_2$

Dissertação constituída por artigo apresentada à Faculdade de Odontologia de Bauru da Universidade de São Paulo para obtenção do título de Mestre em Ciências no Programa de Ciências Odontológicas Aplicadas, na área de concentração em Reabilitação Oral.

Orientador: Prof. Dr. José Henrique Rubo

Coorientadora: Prof. Dr. Ana Flávia Sanches Borges

BAURU

2020

Silva, Lucas José de Azevedo
Synthesis, characterization and mechanic evaluation of dense bovine hydroxyapatite ceramics with $TiO_2$ nanoparticles / Lucas José de Azevedo Silva. -- Bauru, 2020.

45 p. : il. ; 31 cm.

Dissertação (mestrado) -- Faculdade de Odontologia de Bauru, Universidade de São Paulo, ano de defesa.

Orientador: Prof. Dr. José Henrique Rubo

FOLHA DE APROVAÇÃO

# DEDICATÓRIA

Dedico a minha dissertação inicialmente a Deus. Somente com a fé n'ele, e esperança de dias melhores após dias difíceis, tive forças para trilhar um caminho que prometia dificuldades, renúncias, muita dedicação.

Dedico ainda a meus pais, minha base de educação e vida. Pai e mãe, cada um de seu jeito distinto, que convergiram para me educar e me fazer o humano que me tornei hoje. Que se esforçaram para me proporcionar todos os momentos que vivi até hoje. Que sonharam meus sonhos comigo. Que torcem pela minha felicidade e meu sucesso. Que estão comigo em pensamento, mesmo estando distantes fisicamente.

# AGRADECIMENTOS

Agradeço inicialmente aos meus pais, **José de Azevedo Silva** e **Edna Maria da Silva**, que como professores universitários, plantaram em mim desde o inicio da minha vida a importância da busca interminável pelo conhecimento e pelo aprendizado, e que nunca tenha medo e desista frente às adversidades.

À minha irmã, **Anna Angélika**, que embora afastados, sempre foi uma das pessoas fundamentais para a minha educação e para a minha felicidade. A amo.

À **Nitinha**, minha segunda mãe, que sempre se dedicou de forma incansável à minha criação, renunciando por muitas vezes a si mesma. Que sempre me amou como filho e me deu todo o carinho durante toda a minha vida, desde que me entendo por gente.

À **Matheus**, que compartilhou ótimos momentos comigo, entrou pela porta, pegou na minha mão e segurou meus momentos de angustia e ansiedade. Me deixou tranquilo, ajudou, conversou e me fez ver que nem tudo é perfeito, mas que tudo é muito mais fácil do que parece se nós realmente quisermos que seja e fizermos por onde. Estar em Bauru é muito melhor graças a você.

Agradeço aos meus amigos de vida, **Ana Priscila Dias, Camila Carreras, Camila Lopes, Daniel Sousa, Fernanda Vilela, Giovana Moura, Isabeli Góis, Luana Azevedo, Luana Cardoso, Maria Beatriz, Maria Clara, Mariana Borges, Mariana Freitas, Mariana Maia, Marianny Barreto, Raissa Melo, Thayná Rosado**. Cada um deles esteve em algum momento especial e importante da minha vida. Eles também foram responsáveis pelo meu crescimento, entenderam minha ausência e distancia de minha cidade natal, me deram força, amor, carinho, além de comemorarem comigo a cada conquista e sonho alcançados.

Aos meus amigos do Curso de Graduação em Odontologia da UFRN. Foram 4 anos e meio de muito aprendizado e crescimento juntos. Foi lá que nasceu o Lucas dentista de hoje. **Ana Beatriz Arrais, Anna Leticia Lima, Emmily Farias, Fernanda Fagundes, Humberto Chaves, Larissa Luz, Lidya Nara Araújo, Victor Farias, Roberto Fagner**, vocês também fizeram parte da minha formação.

Aos **mestres do Departamento de Odontologia da UFRN**, vocês me deram muito mais do que a base para o que eu Cirurgião-Dentista (quase mestre) de hoje. Defendo e sempre defenderei minha casa, o DOD/UFRN.

Aos **meus colegas de especialização da PROFIS**, cada módulo, conhecimento e sofrimento no vai-e-volta de suas cidades. Sejam de Natal, Belém, Manaus, Cataguazes, Vitória, Bauru, Fortaleza e Rio de Janeiro, cada um com seu conhecimento impar, força para alcançar suas metas e sonhos, enfrentar as dificuldades. **Aline, André, Anna Clara, Everardo, Jefferson, Joaquim, Maria Eduarda, Mariana, Victor e Renan**, amigos que ficarão para sempre em minha vida, que compartilharam as dificuldades durante a especialização.

Ao **Prof. Dr. José Henrique Rubo**, meu orientador, agradeço por ter me recebido de braços abertos e por acreditar no meu potencial. Com sua competência, generosidade, ética, grande paciência e dedicação, o senhor foi essencial para a minha formação.

À **Profª Drª Ana Flávia Sanches Borges**, minha co-orientadora, muito obrigado pelo acolhimento no Departamento de Materiais Dentários e por me fazer um pouco de “materiano” também. Obrigado pela calma e pelos freios nos momentos de muito café no sangue. Obrigado por ser a professora que és.

À **Faculdade de Odontologia de Bauru – USP**, em nome do **Prof. Dr. Carlos Ferreira dos Santos**, diretor da FOB. Agradeço essa casa que me acolheu e que agora posso dizer que também é a minha casa.

Ao **Departamento de Prótese da FOB-USP**, representado pela Profa. Dra. Ana Lúcia Pompéia Fraga de Almeida, fazendo-se membro junto aos professores doutores: **Accácio Lins do Valle, Carlos dos Reis Pereira de Araujo, Estevam Augusto Bonfante, Gerson Bonfante, Karin Hermana Neppelenbroek, Lucimar Falavinha Vieira, Luiz Fernando Pegoraro, Paulo César Rodrigues Conti, Pedro César Garcia de Oliveira, Renato de Freitas, Simone Soares, Vinícius Carvalho Porto e Wellington Cardoso Bonachela**. Agradeço pelo compartilhamento de experiências e conhecimentos.

Aos funcionários da Faculdade de Odontologia de Bauru, principalmente às funcionárias **Cleide e Deborah** do departamento de Prótese, e à **Hebe**, que sempre estiveram à postos para nos ajudar nesses anos de pós-graduação.

Aos colegas de pós-graduação do departamento de prótese, que compartilham a luta diária durante o mestrado e doutorado. Agradeço a companhia dos colegas da minha turma, **Anna Clara, Carolina (Carolzinha) Dyane, Jefferson, Guilherme, Isabel, Isadora, Karina, Lucas, Mariana e Pedro**. Não posso esquecer dos meus colegas que sonharam a entrada nesse curso e estudaram na reta final junto comigo: **Anna Clara, Jefferson e Mariana**. Aqueles dias foram difíceis, mas nos fizeram estar aqui onde estamos hoje. Principalmente à **Anna Clara** que além de tudo compartilhou o mesmo teto e todos os momentos bons e ruins comigo durante esses dois anos. Com certeza sem vocês eu não estaria aqui.

Aos meus amigos da nossa “republica norte-nordeste” que fizeram todos os os momentos mais leves: **Carol, Everardo, Jéssica, Kalil, Mariana, Olga, Rod**. Todos nos ajudamos nos momentos que sentimos falta dos lugares de onde viemos.

À **Brunna Ferrairo**, colega de pesquisa de todos os momentos. Sem a sua companhia, compartilhamento de dúvidas, ajuda braçal e vários outros ensinamentos sobre nossas pesquisas.

Aos pacientes que foram reabilitados na Clínica de Pós-Graduação de Reabilitação Oral da FOB/USP, especialmente a **Sr. Edson Macorin**, que teve minha companhia semanal, paciência e carinho para com todos que nos arrodeavam, em nome dele, agradeço a todos os meus pacientes de Reabilitação.

Agradeço ainda às agencias de fomento à pesquisa do nosso país, **CAPES, CNPq e FAPESP**. O presente trabalho foi realizado com o apoio da Coordenação de Aperfeiçoamento de Pessoal de Nivel Superior – Brasil (CAPES) – **Código de Financiamento 001** e auxilio FAPESP nº **2018/23639-0.**

*“A vida é o que acontece quando se está fazendo planos*”

John Lennon

# ABSTRACT

Bovine bone can be considered a renewable source of hydroxyapatite (HA) for use as a raw material. Recycled bovine bone have the advantages of reducing costs and developing a safe material from a biological source, being a sustainable product, already used in medical and dental treatments. The study aimed to synthesize and characterize the microstructure and mechanical properties of dense bovine hydroxyapatite (HA) ceramics with addition of 5% or 8% of $TiO_2$ nanoparticles in the rutile phase after the final sintering. The structural characterization was obtained from analysis by FTIR, XRD, SEM, EDS and relative density. The mechanical characterization was performed by measuring the fracture toughness after a three-point flexural strength test. The results of the microstructural characterization show that there was no secondary phase formation and that there was a non-homogeneous dispersion of nanoparticles in the HA matrix. The relative density was 2.9 ± 0.09 g/cm3 for HA/8%$TiO_2$np presenting higher density compared with pure HA (2.7 ± 0.03 g/cm3) ($p = 0.011$) and HA/5%$TiO_2$np (2.7 ± 0.05 g / cm3) ($p = 0.041$) groups. Regarding mechanical properties, the flexural strength indicates that pure HA (51.7 ± 10.3 MPa) and HA/8%$TiO_2$np (47.4 ± 6.4 MPa) presented statistically significant different higher results ($p < 0.001$) relative to HA/5%$TiO_2$np group (28.8 ± 3.1 MPa). Such results lead to a fracture toughness value with statistical significance difference between the groups. The pure HA (0.43 ± 0.01 MPa $m^{1/2}$) and HA/8%$TiO_2$np (0.40 ± 0.06 MPa $m^{1/2}$) groups presented higher KIc, comparing with the HA/5%$TiO_2$np group (0.23 ± 0.02 MPa $m^{1/2}$) ($p < 0.003$; $p < 0.007$). It is concluded in this way, that the addition of $TiO_2$ nanoparticles in the rutile phase, through the adopted synthesis methodology, did not manage to increase the fracture toughness results of dense hydroxyapatite ceramics.



**Keyword:** Durapatite, Biocompatible material, Ceramics

# RESUMO

O osso bovino pode ser considerado uma fonte renovável de hidroxiapatita (HA) para uso como matéria-prima. Sua reciclagem tem como vantagens a redução de custos e o desenvolvimento de material seguro a partir de fonte biológica, sendo um produto sustentável, já utilizado em tratamentos médicos e odontológicos. O estudo teve como objetivo sintetizar e caracterizar as propriedades microestruturais e mecânicas das cerâmicas de hidroxiapatita bovina densa (HA) com adição de 5% ou 8% de nanopartículas de $TiO_2$ na fase rutílica após a sinterização final. A caracterização estrutural foi obtida a partir da análise por FTIR, DRX, MEV, EDS e densidade relativa. A caracterização mecânica foi realizada medindo a tenacidade à fratura após um teste de resistência à flexão de três pontos. Os resultados da caracterização microestrutural mostram que não houve formação de fase secundária e que há uma dispersão não homogênea de nanopartículas na matriz HA. A densidade relativa foi de 2,9 ± 0,09 g / cm3 para HA / 8% TiO2np, apresentando maior densidade em comparação com o HA puro (2,7 ± 0,03 g / cm3) (p = 0,011) e o HA / 5% TiO2np (2,7 ± 0,05 g / cm3) (p = 0,041) grupos. Quanto às propriedades mecânicas, os resultados da resistência à flexão indicam que a HA pura (51,7 ± 10,3 MPa) e a HA / 8% TiO2np (47,4 ± 6,4 MPa) apresentaram maior resistência à flexão, com diferença estatisticamente significante (p <0,001) em relação ao grupo HA / 5% TiO2np (28,8 ± 3,1 MPa). Tais resultados levam a um valor de tenacidade à fratura com diferença de significância estatística entre os grupos. Os grupos HA puro (0,43 ± 0,01 MPa m1 / 2) e HA / 8% TiO2np (0,40 ± 0,06 MPa m1 / 2) apresentaram KIc mais alto, comparados com o grupo HA / 5% TiO2np (0,23 ± 0,02 MPa m1 / 2) (p <0,003; p <0,007). Conclui-se, assim, que a adição de nanopartículas de TiO2 na fase rutílica, através da metodologia de síntese adotada, não conseguiu aumentar os resultados de tenacidade à fratura de cerâmicas de hidroxiapatita densa.



**Palavras-Chave:** Durapatita, Materiais biocompatíveis, Cerâmica

# SUMÁRIO

# 1 INTRODUCTION

# 1 INTRODUCTION

The global development process has been accompanied by an increasing trend of solid waste production. Without properly defined recycling processes, incorrect disposal can lead to environmental problems. [1, 2] Thus, bone and meat produced from animal waste deserve important attention in their management [3,4]

The reuse of discarded bovine bone after slaughtering, when properly controlled, can be considered a renewable source of hydroxyapatite (HA) for use as raw material [5,6]. The use of bone residues as raw material for HA extraction is considered solid waste recycling. This procedure has, as main advantages, the reduction of the high cost associated with producing synthetic HA and the supply of a safe material from a biological source, developing a sustainable product [7,8].

Hydroxyapatite is a biomaterial that is already applied clinically for medical and dental treatment. It is considered the main constituent of human bones and teeth [5,6] and characterized by being chemically and directly attached to bone when implanted [9]. Its molecular formula $Ca_{10}(PO_4)_6(OH)_2$ and crystalline structure constitute one of its most important properties, which is the ease of cationic and anionic substitutions [10,11]. These characteristics allows its use as an efficient biocompatible material for use as implants and prostheses [12,13].

HA is already used in dentistry in order to prevent bone loss after tooth extraction, as well as to recover areas with bone resorption. However, it cannot be recommended in situations where heavy loads are present due to its low mechanical resistance, such as fracture toughness, thus being characterized as a fragile material [14-16].

The addition of microstructural reinforcements has already been made with the aim of future fabrication of a polycrystalline ceramic with favorable mechanical properties for a broader use. This methodology has been done as an attempt to mechanically improve composite materials based on synthetic HA. Such mechanical reinforcements act through the control of density and microstructure [17-18]. Therefore, the microstructural characterization of the experimental materials is

necessary to verify the possible formation of new secondary phases. These can be the byproduct from the mixing of the matrix with the reinforcing particles.

The use of reinforcement particles can also cause crack deviation and deflection, leading to a decrease in local maximum stress and crack energy absorption, which may result in the elimination of stress concentration at its tip [19-21]. Such mechanisms act to increase an intrinsic property of materials: fracture toughness.

The stress intensity factor (K) is a measure of the amount of stress concentration that occurs at the tip of a crack previously existing in the material. This measurement is dependent on the applied stress and the geometry and size of this previous crack. By increasing the applied stress, the K increases to a critical point (Kc) where crack propagation occurs until catastrophic failure occurs in the material under study. [22]

Considering the failure mode commonly associated with fragile materials (mode I or opening) we have the representation of fracture toughness by KIc. Thus, KIc represents the fracture toughness corresponding to the amount of energy a material can absorb before catastrophic failure in failure mode I. [22,23]

Among the materials used as reinforcing agents for HA are zirconia, alumina, mullite, titanium, bioglass and ion addition in solid solution in HA [17,18,24-28]. Current studies have used inorganic nanocrystalline metal oxides as a reinforcement mechanism [29-34], suggesting that the addition of these particles would be one of the following ways in search of increased mechanical properties, specifically the fracture toughness of materials.

Meira, 2017, obtained satisfactory results in fracture toughness of HA dense ceramic of bovine origin by adding alumina whiskers as reinforcement [29]. Pires, 2019 [35], used diversified concentrations of ZnO and $TiO_2$ nanoparticles and $TiO_2$ nanotubes as reinforcement for HA and better results were found in the groups with addition of $TiO_2$ nanoparticles.

$TiO_2$ is considered a good option as a nanoparticle added to ceramics [36-39] and has advantages such as good stability [36,37] and applications such as photocatalysis and antimicrobial activity [36-39], besides having significant

biocompatibility [39]. There are four polymorphic phases of $TiO_2$ found in nature: anatase (tetragonal), brookite (orthorhombic), rutile (tetragonal) and $TiO_2$ (B) (monoclinic) [39,40]. However, only the rutile and anatase phases can play some role in $TiO_2$ applications [39] and currently these two phases have been prepared in the form of powders, crystals, thin films, nanotubes and nanoparticles [40].

The rutile phase in relation to the other $TiO_2$ phases is considered the most stable [39,40] at most temperatures and pressures up to 60 Kbar [40]. It can be considered a viable alternative as a nanostructure to obtain mechanical characteristics favorable for a new dense polycrystalline ceramic based on bovine hydroxyapatite.

According to the dental ceramic's latest classification for clinical indications [41], current polycrystalline ceramics can be used in dentistry for copings, anterior and posterior total crowns, up to three-element fixed partial dentures and abutments, as well as dental implant material [37]. The manufacture of bovine

HA polycrystalline dense ceramics is a potential method for reuse of solid waste, reducing the environmental impact caused by its improper disposal, as well as providing a promising, low cost and sustainable biocompatible material for the dental area, by adding intrinsic compositional characteristics, if biological characteristics can be maintained and mechanical properties improved.

# 2 ARTICLE

# 2 ARTICLE

## DENSE POLYCRYSTALLINE BOVINE HYDROXYAPATITE BIOCERAMICS WITH $TIO_2$ RUTILE NANOPARTICLES: SYNTHESIS, NANOSTRUCTURAL AND MECHANICAL CHARACTERIZATION.

Azevedo-Silva LJ[a], Ferrairo BM[a], Pires LA[b], Padovini DSS [C], Dias LFG[d], Erbereli R[e], Fortulan CA[e], Lisboa-Filho PN[d], Borges AFS[b], Rubo JH[a]

a- Department of Prosthodontics and Periodontology, University of São Paulo – Bauru School of Dentistry, Bauru, SP, Brazil

b- Department of Dentistry, Endodontics and Dental Materials, University of São Paulo – Bauru School of Dentistry, Bauru, SP, Brazil

c- Department of Chemistry, São Paulo State University – School of Sciences, Bauru, SP, Brazil

d- Department of Physics, São Paulo State University – School of Sciences, Bauru, SP, Brazil

e- Department of Mechanical Engineering, University of São Paulo – São Carlos Engineering School, São Carlos, SP, Brazil

## ABSTRACT

Recycled bovine bone can be considered a renewable source of hydroxyapatite (HA) for its use as raw material. This procedure has, as main advantages, the reduction of costs and the development of a safe material from a biological source, being a sustainable product, already used in medical and dental treatments. The study aimed to synthesize and characterize the microstructure and mechanical properties of dense bovine hydroxyapatite (HA) ceramics with addition of 5% or 8% of $TiO_2$ nanoparticles in the rutile phase after final sintering. The structural characterization was obtained from analysis by FTIR, XRD, SEM, EDS and relative density. The mechanical characterization was performed by measuring the fracture toughness after a three-point flexural strength test. The results of the microstructural characterization show that there was no secondary phase formation and that there is a non-homogeneous dispersion of nanoparticles in the HA matrix. The relative density was 2.9 ± 0.09 g/cm3 for HA/8%$TiO_2$np presenting higher density compared with the pure HA (2.7 ± 0.03 g/cm3) ($p = 0.011$) and the HA/5%$TiO_2$np (2.7 ± 0.05 g / cm3) ($p = 0.041$) groups. Regarding mechanical properties, the flexural strength results indicate statistical significance difference between the pure HA (51.7 ± 10.3 MPa) and HA/8%$TiO_2$np (47.4 ± 6.4 MPa), presenting higher flexural strength ($p <0.001$) when compared to the HA/5%$TiO_2$np group (28.8 ± 3.1 MPa). Such results lead to a fracture toughness value with statistical significance difference between the groups. The pure HA (0.43 ± 0.01 MPa $m^{1/2}$) and HA/8%$TiO_2$np (0.40 ± 0.06 MPa $m^{1/2}$) groups presented higher KIc, comparing with the HA/5%$TiO_2$np group (0.23 ± 0.02 MPa $m^{1/2}$) ($p <0.003$; $p <0.007$). It was concluded, that the addition of $TiO_2$ nanoparticles in the rutile phase, through the adopted synthesis methodology, did not increased the fracture toughness results of dense hydroxyapatite ceramics.


Keyword: Durapatite, Biocompatible material, Ceramics

## 1 INTRODUCTION

The controlled use of bovine bone use can be considered a renewable source of hydroxyapatite (HA) as raw material [5,6]. The use of organic waste as a raw material for HA extraction is considered solid waste recycling, with some advantages as cost reduction compared to synthetic HA and supply of a safe material from a biological source, developing a sustainable product [7,8].

In attempt to produce a new polycrystalline bioceramic material from bovine HA, a dense bovine HA bioceramic was produced with some interesting charactheristics: 235,2 MPa in biaxial flexural strength test, 335 GPa in Vickers hardness test, $\sigma_0$ and *m* values higher compared to HA bioceramics with nanostructures added [35] and when the pure HA ceramic is compared with pure titanium and commercial zirconia [30], were observed that wettability and roughness tests had similar results between the groups. And also results presented no cytotoxicity and cell adhesion after 24 and 48h.

The use of reinforcement within biomaterials can cause crack deflection and deflection, causing the maximum local stress and energy absorption of the crack, which may cause the tensile stress at its tip to change [19-21]. Among the materials used as reinforcing agents for HA, we highlight zirconia, alumina, mullite, titanium, bioglass and addition of ions in solid solution in HA [17-28]. Pires, 2019 [35], used diverse specimens of ZnO and $TiO_2$ nanoparticles and $TiO_2$ nanotubes as reinforcement for bovine HA and the better results were found in groups with addition of $TiO_2$ nanoparticles.

$TiO_2$ is considered a good choice as ceramic applied nanoparticles [36-39], since it has advantages such as chemical stability [36,37], photocatalysis and antimicrobial performance [36-38], and biocompatibility [39]. $TiO_2$ are in four

polymorphic phases: anatase (tetragonal), brookite (orthorhombic), rutile (tetragonal) and $TiO_2$ (B) (monoclinic) [39,40]. However, only rutile and anatase of analog phases can play some role in $TiO_2$ applications [39] and currently these two phases have been prepared in the form of powders, crystals, thin films, nanotubes and nanoparticles [36]. A rutile phase in relation to the other $TiO_2$ phases is the highest stability considered of [39,40] at most temperatures and pressures up to 60 Kbar [40], introducing itself as a viable alternative to increase mechanical parameters.

According to the classification of dental ceramics based on their clinical indications [41], the current polycrystalline ceramics are indicated for dental treatments such as copings, anterior and posterior crowns, fixed prostheses up to three elements and abutments, as well as dental implant material [42]. Thus, the aim of the present study was to synthesize, characterize and evaluate the influence of the addition of two $TiO_2$ amounts on the microstructure and mechanical properties by fracture toughness of the bovine HA bioceramic as a potential biomaterial for dental implant materials.

## 2 MATERIALS AND METHODS

### *Specimens preparation*

#### *2.1 Preparation of $TiO_2$ nanoparticles by* Arruda, 2015 [43]

Rutile $TiO_2$ nanoparticles were obtained by the sol-gel process. Into an Erlenmeyer flask, 185 ml of distilled water, 56.7 ml of Isopropanol and 2.6 ml of nitric acid ($HNO_3$) were added. After this, 15 ml of titanium (IV) isopropoxide was added to solution and stirred (300 rpm) for 30 min. The solution was heated at 85°C while stirring. These heating and stirring patterns were maintained until complete evaporation of the liquid, resulting in crystallization. Afterwards, it was taken to the furnace to reduce the homogeneous powder.

### *2.2 HA powder preparation*

The materials used in the manufacture of experimental ceramic were polyvinyl butyral (PVB) (Butvar B98) as a binder, 4-aminobenzoic acid (PABA) as deflocculant and isopropyl alcohol as the solvent of the binder as well as liquid barbotine medium (Table 1).

Bovine (2 years old) metatarsus specimens, passed by an initial manual cleaning, then, went through thermochemical processes for removal of residual organic matter [44]

Following the production of particulate hydroxyapatite, in the alcoholic environment two types of milling were performed. At the first milling, the jar was loaded with 30 vol% Hydroxyapatite, 69.95 vol% isopropyl alcohol and 0.05 wt% PABA (para-aminobenzoic acid). The mix was placed in a rotatory mill for 48 hours and after, for 96 hours vibrating in ball mill.

After this period, 1.2% by weight of PVB (polyvinyl butyral) dissolved in isopropanol was added and homogenized in the vibratory mill for two hours. For specimens with nanomaterials, after these two hours in the vibrating mill, the $TiO_2$ nanoparticles were weighed at 5% and 8% of the working volume relative to HA and added to a smaller HA-loaded jar. The mixture was returned to the vibrating mill for 10 minutes.

After the second mill, each jar was discharged and the barbotine was dried with a hot air blower at about 80°C. This mixture was granulated in sieves # 200 mesh ≤ 75 μm to obtain granules average size of 35 μm.

### *2.3 Ceramic bars preparation*

The experimental groups were: pure HA, HA/$TiO_2$np5% and HA/$TiO_2$np8% (5 and 8% of $TiO_2$ nanoparticles)

For specimen preparations, 1.5 g of the powders were weighed, inserted into a rectangular device, generating the conformation of specimens with 21mm length x 4 mm width x 3 mm height, after uniaxial pressing 100 MPa for 1 minute. The specimens were beveled using a metal device, where the four largest edges of each specimen were beveled to a standard width of 0.1mm in accordance with ISO 6872 (2015) [45].

The specimens were pressed by isostatic press at 200 Mpa for 1 minute. The sintering process were carried out in a Lindberg Blue / M chamber-type furnace in an air atmosphere from room temperature to 160°C at a heating rate of 2.7 ° C/min, then to 600°C at 4°C/min., then to 1100°C at 5°C/min and finally at the maximum temperature (1300°C) at 6°C/min, with a level of 120 minutes followed by slow oven cooling to room temperature.

### ***Structural analyses***

### *2.4 X-ray Diffraction (XRD)*

Specimens and powder were positioned in the specimen holder to ensure a smooth surface and mounted on a fixed horizontal specimen plane. Spectra were recorded at room temperature on a Philips X' Pert X-ray diffractometer with a Cu Kα source (λ=1.5418 Å) in Bragg–Brentano geometry (2θ). Data analyses were carried out using profile fits of select individual XRD peaks.

### *2.5 Fourier Transform Infrared Spectroscopy (FTIR)*

Ceramic powders sintered specimens were submitted to spectroscopy on infrared frequency (Vertex 70, Bruker). In the present work, this technique observed the vibration bands that occur between 4000 and 400 cm-1.

### *2.6 Field Emission Scanning Electron Microscope (FE-SEM)/Energy Dispersive Spectroscopy (EDS)*

Five specimens from each group was randomly selected after tests and then gold-sprayed for scanning electron microscopy (SEM) analysis (ZEISS, Supra40, Jena, Germany). The measurements were taken into fractured surfaces in 80x, 200x, 400x and 3.000x of magnification.

Five specimens from each group was randomly selected after tests and then gold-sprayed for scanning electron microscopy (SEM) analysis (ZEISS, Supra40, Jena, Germany). The composition measurements were taken in 3.000x magnification at external and fractured surfaces in bar specimens and in start powders.

### *2.7 Relative Density (n=10)*

The relative density measurement procedure was performed by the Archimedes principle. This methodology requires mass measurements under 3 different conditions for each specimen: (1) Dry measurement, (2) wet specimens and (3) in liquid immersion.

Density values are obtained with the following equation for each specimen:

$$\rho_{specim} = \frac{w_S}{(w_U - w_I)}\ x\ \rho_{liquid}$$

Where: ρ specimen is the specimen density, $w_S$ is the dry specimen weight, $w_U$ is the wet specimen weight, $w_I$ is the liquid immersion specimen weight, and ρ liquid is the density of the liquid used for specimen immersion.

Mechanical analyses

***2.8 Flexural strength*** *(n=10)*

The 3-point flexural strength test (σf) of the bar specimens was performed on a universal testing machine (Sintec 5G, MTS) with a 5000 N compression load and a constant speed of 0.5mm / min. The specimens were positioned in a 3-point flexure device with a distance of 12.0 mm between the support cylinders and the center of the metal sphere where the load was applied. The flexural strength values (σf) were determined according to the equation: $\sigma_f = 3Pl / 2wb^2$, where P is the fracture load (N), l is the distance between the supports (span) (12 mm), w is the specimen width (mm), and b is the specimen thickness (mm).

***2.9 Fracture toughness by flexural surface fracture (FSF)*** *(adapted from Cesar, et al., 2017 [22], Ramos et al., 2016 [46]) (n=10)*

Fractured specimen surfaces were cleaned in detergent solution for 15 minutes immersed in ultrasound, followed by immersion for 15 minutes in deionized water and 100% ethanol bath. Specimen surfaces were first examined under a stereomicroscope (Leica 0.45X, Meiji Techno, Japan) to determine the location of the fracture origin.

The size of the critical defect (c) was measured (Image J, Wayne Rasband, USA) at 200x magnification, and quantitative analysis was conducted based on the equation:

$c=(ab)^{1/2}$, where (a) is the height of the origin of the defect and (b) is half its width [47]

The fracture toughness (KIc) was estimated using the flexural strength values (σf) by applying the fracture mechanical principles. The equation: KIc = Yσ_f √a was used for the calculation, based on Griffith – Irwin theory [48,49] where KIc is fracture toughness (MPa.m1 / 2), σf is resistance to fracture (MPa), Y is the geometric factor of stress intensity (related to defect geometry), and c is the defect size. Y is the parameter that considers the location and shape of the initial defect, which will be calculated according to ASTM C1421.

### *2.10 Statistical analyses*

Data were submitted to the Kolmogorov-Smirnov and Shapiro-Wilk normality tests. The Levene test was performed to verify the homogeneity of the variances. After verification of normality, they were analyzed by ANOVA at α = 0.05, followed by Tukey post-test for comparison between groups.

## 3 RESULTS

### *3.1 X-Ray diffraction (XRD)*

The XRD results are shown in Figure 2. The XRD spectrum identified predominance in crystallographic planes characteristics of Hydroxyapatite (Card No.: 00-009-0432). The presence of $TiO_2$ rutile phase peeks is also observed (Card No.: 00-002-0494), in a secondary, tenuous but defined, because of its low amount in the hydroxyapatite matrix. The co-existence of HA and $TiO_2$ can also be observed in specimens with the addition of nanoparticles. Therefore, there was no creation of a secondary phase.

### *3.2 Fourier Transform Infrared Spectroscopy (FTIR)*

The FTIR results shows the chemical bonds present in the materials with the bonds represented in graphs (Figure 3 and 4). In all specimens, it can be noted bands attributed to $PO_4^{3-}$ groups (1101, 1026, 633 and 560 $cm^{-1}$). The band at 1650 $cm^{-1}$ is attributed to $H_2O$ bonds. The band at 2300 $cm^{-1}$ is attributed to atmospheric $CO_2$, and at 1545 $cm^{-1}$, attributed to the $CO_3^{2-}$ ions. This can be caused by the dissolution of atmospheric $CO_2$ in the synthesis [50]. The band 2010 $cm^{-1}$ is attributed to $Ca^{2+}$-CO bond [51].

The $TiO_2$ rutile nanoparticles can be noticed by the Ti-O-Ti and Ti-O bonds from 450 to 500 $cm^{-1}$ [52]. As also seen in the XRD results, there was no link between Ti and any chemical element present in HA.

Regarding the graph with sintered materials, it can be noticed a stretched 1100 cm-1 band in the sintered specimens, made possible by absorbed water. This pattern is not seen in the sintered specimens. The Ti-O-Ti and Ti-O bonds is only evidenced in the sintered specimen of 5% $TiO_2$ added. In the other specimens, these bands may be deviated to a frequency below 500 cm-1. According to the literature, such connections can be observed from 400 to 700 cm-1 [52].

### *3.3 Field Emission Scanning Electron Microscopy (FE-SEM)/ Energy Dispersive Spectroscopy (EDS)*

The FE-SEM images (3000× magnification) of fracture surface, shows a surface similarity between the pure HA group and the group with 8% $TiO_2$ added (Figures 5a and 5c). The group with 5% of nanoparticles (Figure 5b) shows its surface with a greater disorganization of the grains, presenting a fracture pattern apparently different

from the others. We can also notice an apparent greater cohesion between the grains of the specimens of pure ceramics and with the addition of 8% of TiO2 nanoparticles.

Another characteristic that can be noticed is the reduction of pores in the groups with the addition of nanoparticles in relation to the group without $TiO_2$. The group with 5% $TiO_2$ nanoparticles appears to have a lower number of pores when compared to the others.

The EDS analyses are presented in Figures 6, 7 and 8. The results of defined localization indicate the composition of the material. The chemical elements saw were calcium, phosphorus, oxygen, magnesium and gold for all groups. Moreover, titanium was identified for reinforced $TiO_2$ nanoparticles groups.

For the defined location, the EDS mapping (Figures 9 and 10) shows the irregularity in the distribution of Ti in the specimen, both in the group 5% and in the 8% reinforced $TiO_2$ nanoparticles groups.

### *3.4 Relative Density*

The relative density values are presented in Table 2. The results indicate statistically significant difference between the groups. The HA/$TiO_2$np8% group (2,9± 0,09 g/$cm^3$) presented higher density compared with the pure HA (2,7± 0,03 g/$cm^3$) (p= 0,011) and the HA/$TiO_2$np5% (2,7± 0,05 g/$cm^3$) (p= 0,041) groups. The pure HA and HA/$TiO_2$np5% groups presented statistical similarity in their results (p=0,735).

### **3.5** ***Flexural Strength (FS)***

The flexural strength data obtained from 3-point surface flexion are presented in Table 3. The results indicate statistical significance difference between the groups. The pure HA (51.7 ± 10,3 MPa) and HA/$TiO_2$np8% (47,4 ± 6,4 MPa) groups presented higher flexural strength, being similar to each other (p=0,331). Comparing with the

HA/$TiO_2$np5% group (28,8 ± 3,1 MPa), the previously mentioned groups presented significant difference (p<0,001; p<0,001).

### 3.6 *Fracture Toughness by flexural surface fracture (FS)*

The Fracture Toughness (KIc) and critic defect (c) data obtained are presented in Table 4. The results indicate statistical significance difference between the groups. The pure HA (0,43 ± 0,01 MPa $m^{1/2}$) and HA/$TiO_2$np8% (0,40 ± 0,06 MPa $m^{1/2}$) groups presented higher KIc, being similar to each other (p=0,849). Comparing with the HA/$TiO_2$np5% group (0,23 ± 0,02 MPa $m^{1/2}$), the previously mentioned groups presented statistically significant difference (p<0,003; p<0,007).

## 4. DISCUSSION

The proposal of the study was the synthesis of a reinforced hydroxyapatite dense bioceramic with 5 and 8% of $TiO_2$ nanoparticles. Characteristics are sought between the mimetic, tooth, and the purely mechanical ideal, with high hardness, such as Zirconia.

Following a previous study [35] that found promising results by adding $TiO_2$ nanoparticle in a HA matrix comparing to pure HA ceramic, this kind of nanostructure was chosen in attempts to increase some mechanical properties. The choice of higher amount in $TiO_2$ nanoparticle was followed. It was assumed that a crack deflection mechanism, reported by Faber and Evans [19], could be increase the reinforced HA groups material fracture toughness. The choice for rutile $TiO_2$ nanoparticle was based on its greater chemical stability in comparison to anatase $TiO_2$ [39,40]. It can be noticed through the FTIR and XRD analyzes the incorporation of $TiO_2$ nanoparticles as a load

particle in the two groups with the $TiO_2$ nanoparticles added. In the present work, the mix of hydroxyapatite and $TiO_2$ nanoparticles did not form secondary phases. However, the EDS analysis shows that the titanium distribution in the specimens was not homogeneous, however, HA/$TiO_2$np8% showed be more homogeneous than HA/$TiO_2$np5%. The irregularity in the distribution of $TiO_2$ may be one of the reasons why the mechanical properties of the HA/$TiO_2$np5% was lower compared to the others groups in both, flexural strength and fracture toughness properties.

The second reason can be the absence of secondary phases with HA, since the location in the matrix can influence the material's resistance. The reinforcement particle can be distributed in four modes: 1) along the grain boundaries of the matrix, 2) inside the grains of the matrix, 3) both along the grain boundaries or inside the grains, or 4) both the matrix and reinforcement grains are uniformly distributed [53]. If they are uniformly distributed in the material matrix, they behave differently than they do when are concentrated in the grain's insides or boundaries, resulting in a material with better mechanical properties [54]. Moreover, the nanostructure being along the grain boundaries is one of the reasons for the easy fracture of the composite material [53]. However, as the more uniform distribution was seen for HA/$TiO_2$np8% the major localization of nanoparticles in our materials matrix was more seemed to be in the grain boundaries, further analyses can be conducted to exactly determine this in ceramic composites as SEM, TEM, Laser Confocal Microscopy, Raman spectrocopy and Zeta potential analyses [53].

It is also known in the literature that one of the characteristics of the $TiO_2$ anatase phase is its good behavior when added to ceramic materials [38,55-59]. In the previous study by Pires et al, 2020 [35], in the 5% concentration of Anatase, the

mechanical characteristics of dense HA ceramics are similar to those of pure HA. In this current study, $TiO_2$ rutile resulted in lower mechanical values at a concentration of 5%. Despite the poor flexural strength and fracture toughness shown in the HA with 5% amount of rutile, when this concentration is increased to 8% amount, the results were similar to the pure HA.

Fractographic inspection is needed to perform the fracture toughness analyses [46]. By verifying the fracture origin, size, geometry and characteristic areas that define the critical defect that possibly caused the initial of the fracture [59]. Fractographic can predict the fracture toughness of the ceramic materials from flexural strength tests [58,59]. Regarding the size of the critical defect, similar averages were observed among the groups, showing means of 44.4 μm, 44.0 μm and 40.0 μm, respectively for pure HA, Ha/$TiO_2$5%np and Ha/$TiO_2$8%np. It is important to note that, according to the Griffith–Irwin theory calculation [48,49], the greater the flexural strength and critical defect size, the greater the fracture toughness result.

When the mechanical results are thought related to the relative density results, HA/$TiO_2$np8% still is a promising group. Density results are in accordance to the higher theoretical density of $TiO_2$ [38] since pure HA group and HA/$TiO_2$np5% were similar, being a number between 5 and 8% on which above this increased its density compared to the pure HA. It was defined in previous studies that use mechanical mechanisms such as nanoparticles, can act on density increasing and microstructure control by grain growth of materials [17-18].

Furthermore, another factor that can be inferred through the density result is the number of pores in the material structure. A previous study [61] discussed the possible relation between the pores existing and the grain growth. Its sizes increase with the gas diffusion within pores during sintering process. In addition, the grain growth

increasing, increases the relative density of the material [61]. Other previous literature discusses the increase of the pores number with increase of particles amount. [62,63]. However, it is yet discussed that other factors that influence this fact, such ceramic grain size, grain growth and grain boundaries [64,65]. Moreover, adjusting the correct sintering time and temperature for the material, can also decrease the number of pores [62,63], grain growth and material densification [61].

The homogeneous distribution of the microstructures can influence the sintering process [61]. Usually, when mixing powders, the material can agglomerate resulting in small inter-agglomerated pores. During sintering, they can sinter faster with the rapid growth of grains, while the large inter-clustered pores of the non-clustered matrix have a lower sintering predisposition. [66-68]. Finally, the optimization of the temperature leads to an increase in the bond strength between the grains of the material, which may increase its mechanical strength [62,69,70].

## 5. CONCLUSIONS

Within the limitations of this in vitro study, it can be concluded that:

The addition of rutile $TiO_2$ nanoparticles to an HA matrix can be considered as a filler particle and the 8% in volume can be a promising HA blend material, since flexural strength and fracture toughness similar to the pure HA, and superior relative density.

## REFERENCES


1. Wang F, Cheng Z, Reisner A, Liu Y. Compliance with household solid waste management in rural villages in developing countries. Journal of Cleaner Production, 20 November 2018, Vol.202, pp.293-298
2. Suttibak S, Nitivattananon V. Assessment of factors influencing the performance of solid waste recycling programs. Resources, Conservation & Recycling, 2008, Vol.53(1), pp.45-56
3. Sufian MA, Bala BK. Modeling of urban solid waste management system: The case of Dhaka city. Waste Management, 2007, Vol.27(7), pp.858-868
4. Cascarosa E., Boldrin A. and Astrup T. Pyrolysis and gasification of meat-and-bone-meal: Energy balance and GHG accounting. Waste Management, 2013, Vol. 33, pp.2501–2508.
5. Eanes ED. Crystal-Growth of Mineral Phases in Skeletal Tissues. Prog Cryst Growth Ch. 1980;3(1):3-15.
6. Oguchi H, Ishikawa K, Mizoue K, Seto K, Eguchi G. Long-Term Histological-Evaluation of Hydroxyapatite Ceramics in Humans. Biomaterials. 1995;16(1):33-8.
7. Szabo-Júnior AM. Educação ambiental e gestão de resíduos. 3. ed. São Paulo: Rideel, 2010.
8. Jabbour ABLS, Jabbour CJC. Gestão ambiental nas organizações: fundamentos e tendências. São Paulo: Atlas, 2013
9. Bagambisa FB, Joos U, Schilli W. Mechanisms and Structure of the Bond between Bone and Hydroxyapatite Ceramics. J Biomed Mater Res. 1993;27(8):1047-55.
10. Elliot JC. Structure and chemistry of the Apatites and other Calcium Orthophosphates. Studies in inorganic chemistry. 1. ed.(18). Elsevier Science B.V. 1994
11. Rey C, Combes C, Drouet C, Sfihi H, Barroug A. Physico-chemical properties of nanocrystalline apatites: Implications for biominerals and biomaterials. Mat Sci Eng C-Bio S. 2007;27(2):198-205.
12. Kawachi EY, Bertran CA, dos Reis RR, Alves OL. Bioceramics: Tendencies and perspectives of an interdisciplinary area. Quim Nova. 2000;23(4):518-22.
13. Rodrigues CV, Serricella P, Linhares AB, Guerdes RM, Borojevic R, Rossi MA, et al. Characterization of a bovine collagen-hydroxyapatite composite scaffold for bone tissue engineering. Biomaterials. 2003;24(27):4987-97.
14. Bouslama N, Ben Ayed F, Bouaziz J. Effect of fluorapatite additive on densification and mechanical properties of tricalcium phosphate. Journal of the mechanical behavior of biomedical materials. 2010;3(1):2-13.
15. Ramesh S, Tan CY, Tolouei R, Amiriyan M, Purbolaksono J, Sopyan I, et al. Sintering behavior of hydroxyapatite prepared from different routes. Mater Design. 2012; 34:148-54.
16. Sebdani MM, Fathi MH. Preparation and characterization of hydroxyapatite-forsterite-bioactive glass nanocomposite coatings for biomedical applications. Ceram Int. 2012;38(2):1325-30.
17. Ravarian R, Moztarzadeh F, Hashjin MS, Rabiee SM, Khoshakhlagh P, Tahriri M. Synthesis, characterization and bioactivity investigation of bioglass/hydroxyapatite composite. Ceram Int. 2010;36(1):291-7.
18. Yelten A, Yilmaz S, Oktar FN. Sol-gel derived alumina-hydroxyapatite-tricalcium phosphate porous composite powders. Ceram Int. 2012;38(4):2659-65.

19. Faber KT, Evans AG. Crack deflection processes-I. Theory. Acta Metallurgica. 1983;31(4);565-576.
20. Fortulan, CA. Compósito alumina-zircônia: obtenção atavés de conformação coloidal e caracterização microestrutural [Relatório de Pós-doutorado]. São Carlos: Universidade Federal de São Carlos; 1999.
21. Fang Z, Feng QL, Tan RW. In-situ grown hydroxyapatite whiskers reinforced porous HA bioceramic. Ceram Int. 2013;39(8):8847-52.
22. Cesar PF, Della Bona A, Scherrer SS, Tholey M, van Noort R, Vichi A, et al. ADM guidance-Ceramics: Fracture toughness testing and method selection. Dental materials: official publication of the Academy of Dental Materials. 2017;33(6):575-84.
23. Anusavice KJ, Shen C, Rawls HR. Philips' Science of dental materials. 12th ed. Elsevier/Saunders, 2012.
24. Ramires PA, Romito A, Cosentino F, Milella E. The influence of titania/hydroxyapatite composite coatings on in vitro osteoblasts behaviour. Biomaterials. 2001;22(12):1467-74.
25. Silva VV, Lameiras FS, Domingues RZ. Microstructural and mechanical study of zirconia-hydroxyapatite (ZH) composite ceramics for biomedical applications. Compos Sci Technol. 2001;61(2):301-10.
26. Kalita SJ, Rokusek D, Bose S, Hosick HL, Bandyopadhyay A. Effects of MgO-CaO-P2O5-Na2O-based additives on mechanical and biological properties of hydroxyapatite. J Biomed Mater Res A. 2004;71A(1):35-44.
27. Ning CQ, Zhou Y. On the microstructure of biocomposites sintered from Ti, HA and bioactive glass. Biomaterials. 2004;25(17):3379-87.
28. Nath S, Dey A, Mukhopadhyay AK, Basu B. Nanoindentation response of novel hydroxyapatite-mullite composites. Mat Sci Eng a-Struct. 2009;513-14:197-201.
29. Meira CR. Processamento de hidroxiapatita bovina associada com prototipagem rápida visando implantes ósseos [Tese]. São Carlos: Universidade de São Paulo; 2014.
30. Pires LA, Fortulan CA, Rontani RM, Oliveira RC, Dainezi VB, Oliveira FA, Tokuhara C, Graeff MSZ, Meira CR, Borges AFS. Wettability and pre-osteoblastic behavior evaluations of a dense bovine hydroxyapatite ceramic. Journal of Oral Science, 2019.
31. Fortuny A, Bengoa C, Font J, Fabregat A. Bimetallic catalysts for continuous catalytic wet air oxidation of phenol. J Hazard Mater. 1999;64(2):181-93.
32. Rana S, Rawat J, Sorensson MM, Misra RDK. Antimicrobial function of Nd3+-doped anatase titania-coated nickel ferrite composite nanoparticles: A biomaterial system. Acta Biomater. 2006;2(4):421-32.
33. Cheng LC, Jiang XM, Wang J, Chen CY, Liu RS. Nano-bio effects: interaction of nanomaterials with cells. Nanoscale. 2013;5(9):3547-69.
34. Magalhães APR, Fortulan CA, Lisboa-Filho PN, Ramos-Tonello CM, Gomes OP, Cesar PF, Fukushima KA, Mondelli RFL and Borges AFS. Effects of Y-TZP blank manufacturing control and addition of TIO2 nanotubes on structural realibility of dental materials. Ceramics International, 15 February 2018, Vol.44(3), pp.2959-2967
35. Pires LA, Silva LJA, Ferrairo BM, Erberelli R, Lovo JFP, Ponce O, Rubo JHR, Lisboa-Filho PN, Griggs JA, Fortulan CA, Borges AFS. Effects of ZnO/$TiO_2$ nanoparticle and $TiO_2$ nanotube additions to dense polycrystalline hydroxyapatite bioceramic from bovine bones. Dental materials, v.36, p. E38-E46, 2020.

36. Rahman MM, Krishna KM, Soga T, Jimbo T, Umeno M. Optical properties and X-ray photoelectron spectroscopic study of pure and Pb-doped TiO2 thin films. Journal of Physics and Chemistry of Solids, 1999, Vol.60 (2), pp.201-210.
37. Zhao Y, Li C, Liu X, Gu F, Jiang H, Shao W, Zhang L, He Y. Synthesis and optical properties of TiO2 nanoparticles. Materials Letters, 2007, Vol.61 (1), pp.79-83
38. Diebold U. The surface science of titanium dioxide. Surface Science Reports, 2003, Vol.48 (5), pp.53-229.
39. Gupta SM, Tripathi M. Review of TiO2 nanoparticles. Chinese science bulletin Kexue tongbao, 2011, Vol.56(16), pp.1639-1657
40. Carp O, Huisman C L, Reller A. Photoinduced reactivity of titanium dioxide. Prog in Solid State Chem, 2004, 32: 33–117
41. Gracis S, Thompson VP, Ferencz JL, Silva NRFA, Bonfante EA. A New Classification System for All-Ceramic and Ceramic-like Restorative Materials. Int J Prosthodont. 2015;28(3):227-35.
42. Siddiqi A, Khan AS, Zafar S. Thirty Years of Translational Research in Zirconia Dental Implants: A Systematic Review of the Literature. J Oral Implantol. 2017;43(4):314-25.
43. Arruda LB, Santos CM, Orlandi MO, Schreiner WH, Lisboa PN. Formation and evolution of TiO2 nanotubes in alkaline synthesis. Ceram Int. 2015;41(2):2884-91.
44. Erbereli, Rogério. Avaliação da qualidade óssea de bovinos. [Dissertação]. São Carlos: Escola de Enganharia de São Carlos, Universidade de São Paulo, 2017.
45. International Standard ISO 6872, Dentistry – Ceramic Materials, International Standards Organization, Geneva, Switzerland, 2015.
46. Ramos CM, Cesar PF, Bonfante EA, Rubo JH, Wang L, Borges AF. Fractographic principles applied to Y-TZP mechanical behavior analysis. Journal of the mechanical behavior of biomedical materials. 2016; 57:215-23.
47. 1322-02a AC, 2003. Standard Practice for Fractography and Characterization of Fracture Origins in Advanced Ceramics.
48. Griffith, A.A., 1920. The phenomena of rupture and flow in solids. Philos. Trans. R. Soc. 221, 35.
49. Irwin GR. Analysis of stresses and strains near the end of a crack transversing a plate. J Appl Mech. 1957; 24:361-64.
50. Veiga A, Castro F, Reis C, Sousa A, Oliveira AL, Rocha F. Hydroxyapatite/sericin composites: A simple synthesis route under near-physiological conditions of temperature and pH and preliminary study of the effect of sericin on the biomineralization process. Materials Science & Engineering C, March 2020, Vol.108
51. Pekounov Y, Chakarova K, Hadjiivanov K. Surface acidity of calcium phosphate and calcium hydroxyapatite: FTIR spectroscopic study of low-temperature CO adsorption. Materials Science & Engineering C, 2009, Vol.29(4), pp.1178-1181
52. Huo X, Liu P, Zhu J, Liu X, Ju, H. Electrochemical immunosensor constructed using TiO2 nanotubes as immobilization scaffold and tracing tag. Biosensors and Bioelectronics, 15 November 2016, Vol.85, pp.698-706
53. Saheb N, Qadir NU, Siddiqui MU, Arif AFM, Akhtar SS, Al-Aqeeli N. Characterization of Nanoreinforcement Dispersion in Inorganic Nanocomposites: A Review. Materials, 2014, Vol.7(6), p.4148-4181
54. Yamamoto G, Hashida T. Carbon nanotube reinforced alumina composite materials. In *Composites and Their Properties*; Hu, N., Ed.; InTech: Rijeka, Croatia, 2012.

55. Al-Salim NI, Bagshaw SA, Bittar A, Kemmitt T, McQuillan AJ, Mills AM, Ryan MJ. Characterization and activity of sol–gel-prepared $TiO_2$ photocatalysts modified with Ca, Sr or Ba ion additives, J. Mater. Chem. 10 (2000) 2358–2363.
56. Braun JH. Titanium dioxide: a review. J.Coat.Technol.69(1997)59–72.
57. R.X. Cai, Y. Kubota, T. Shuin, H. Sakai, K. Hashimoto, A. Fujishima, Induction of cytotoxicity by photoexcited $TiO_2$ particles, Cancer Res. 52 (1992) 2346–2348.
58. A. Fujishima, X.T. Zhang, Titanium dioxide photocatalysis: present situation and future approaches, CR Chim. 9 (2006) 750–760.
59. Rice, R.W., 1991. Fractographic determination of $K_{Ic}$ and effects of microstructural stresses in ceramics. Fractography of glasses and ceramics, Ceramic Transactions. American Ceramic Society38 17.
60. Scherrer, S.S., Kelly, J.R., Quinn, G.D., Xu, K., 1999. Fracture toughness ($K_{Ic}$) of a dental porcelain determined by fractographic analysis. Dent. Mater. 15 (5), 342–348.
61. Ju H, Ning K, Lu K. Sintering behaviors of micron-sized ceramic rod features Acta Materialia, 01 February 2018, Vol.144, pp.534-542
62. Miranda RBP, Miranda WG, Lazar DRR, Ussui V, Marchi J,Cesar PF. Effect of titania content and biomimetic coating on the mechanical properties of the Y-TZP/TiO2composite.Dent Mater 2018;34(February (2)):238–45.[36]
63. Miao X, Sun D, Hoo PW, Liu J, Hu Y, Chen Y. Effect of titania addition on yttria-stabilized tetragonal zirconia ceramics sintered at high temperatures. Ceram Int 2004;30(6):1041–7.
64. Cota FP, Alves RAA, Panzera TH, Strecker K, Christoforo AL, Borges PHR. Physical properties and microstructure of ceramic–polymer composites for restoration works. Materials Science & Engineering A, 2012, Vol.531, pp.28-34
65. Bernard-Granger G, Guizard C. New relationships between relative density and grain size during solid-state sintering of ceramic powders. Acta Materialia, 2008, Vol.56(20), pp.6273-6282
66. Maximenko AL, Olevsky EA, Grigoryev EG, Homogenization of biporous agglomerated powder structures during high-temperature consolidation, J. Am. Ceram. Soc. 98 (11) (2015) 3445e3452.
67. Maximenko AL, Olevsky EA, Shtern MB, Plastic behavior of agglomerated powder, Comp. Mater Sci. 43 (4) (2008) 704e709.
68. Li W, Olevsky EA, Khasanov OL, Back CA, Izhvanov O, Opperman J, Khalifa HE. Spark plasma sintering of agglomerated vanadium carbide powder, Ceram. Int. 41 (3) (2015) 3748e3759.
69. Eichler J, Rödel J, Eisele U, Hoffman M. Effect of grain size on mechanical properties of submicrometer 3Y-TZP: fracture strength and hydrothermal degradation. J Am Ceram Soc2007;90(September (9)):2830–6.
70. Stawarczyk B, Özcan M, Hallmann L, Ender A, Mehl A, Hämmerlet C. The effect of zirconia sintering temperature eon flexural strength, grain size and contrast ratio. Clin Oral Investig 2013;17(1):269–74.

## APPENDIX – TABLES AND FIGURES

**Table 1.** Density and proportion of components used in specimens' preparation.

| Component | Density (g/cm$^3$) | Proportion (%) | Function |
|---|---|---|---|
| **HA** | 3.14 | 30% (total volume) | Ceramic powder |
| **PABA (4-Aminobenzoic acid)** | 1.37 | 0.05% ($ZrO_2$ weight) | Deflocculant |
| **PVB (Polyvinyl butyral)** | 1.1 | 2% ($ZrO_2$ weight) | Binder |
| **Isopropyl alcohol** | 0.78 | 70% (total volume) | Solvent |
| **$TiO_2$ nanoparticles** | 4.23 | 5 and 8% (total volume) | Reinforcement |

**Table 2.** Relative Density Data of experimental dense bovine HA ceramics by Archimeds' Method (g/cm$^3$)

| Groups | Mean ± Standard Deviation |
|---|---|
| **HA** | 2,7± 0,03 b |
| **HA/$TiO_2$np5%** | 2,7± 0,05 b |
| **HA/$TiO_2$np8%** | 2,9± 0,09 a |

Different letters indicate statistically significant difference of 5% ($p<0.05$).

**Table 3.** Flexural Strength Data of experimental dense bovine HA (MPa)

| Groups | Mean ± Standard Deviation |
|---|---|
| **HA** | 51.7 ± 10,3 a |
| **HA/$TiO_2$np5%** | 28,8 ± 3,1 b |
| **HA/$TiO_2$np8%** | 47,4 ± 6,4 a |

Different letters indicate statistically significant difference of 5% ($p<0.05$).

**Table 4.** Critical Defect (c) and Fracture Toughness (KIc) Data of experimental dense bovine HA

| | HA | HA/$TiO_2$np5% | HA/$TiO_2$np8% |
|---|---|---|---|
| **c (µm)** | 44,4 | 44,0 | 40,0 |
| **KIc (MPA m$^{1/2}$)** | 0,43 ± 0,01 a | 0,23 ± 0,02 b | 0,40 ± 0,06 a |

Different letters indicate statistically significant difference of 5% ($p<0.05$).

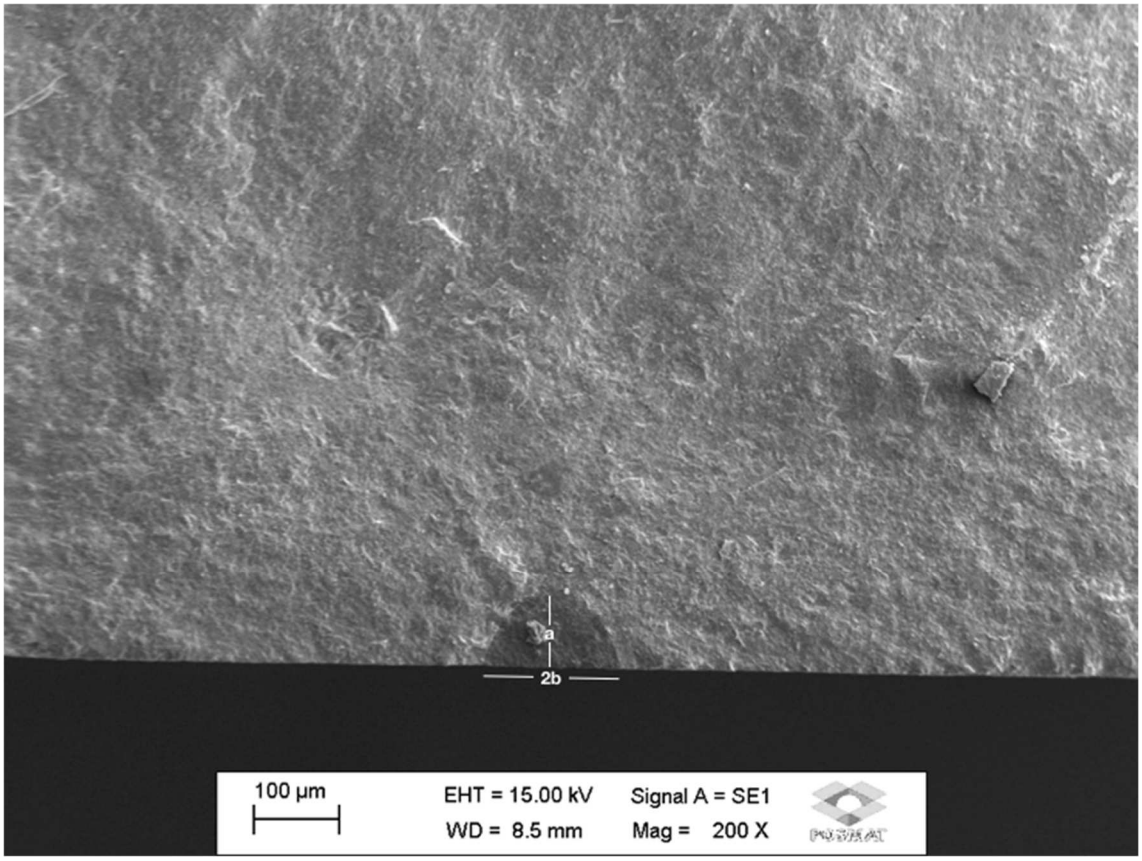


*Figure 1. Fractured surface of pure bovine HA ceramic with schematic critical defect measurement*

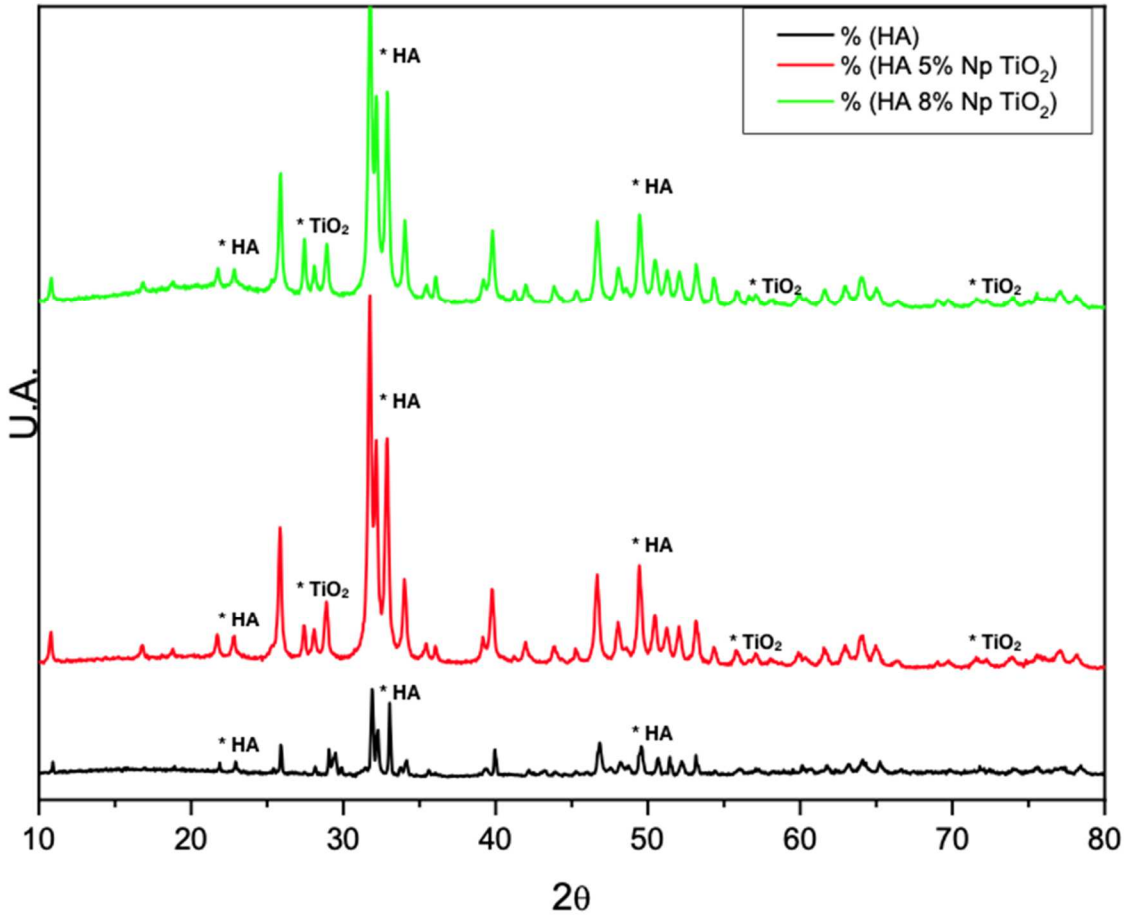


*Figure 2. XRD patterns of pure HA, HA/5%TiO2np and HA/8%TiO2np.*

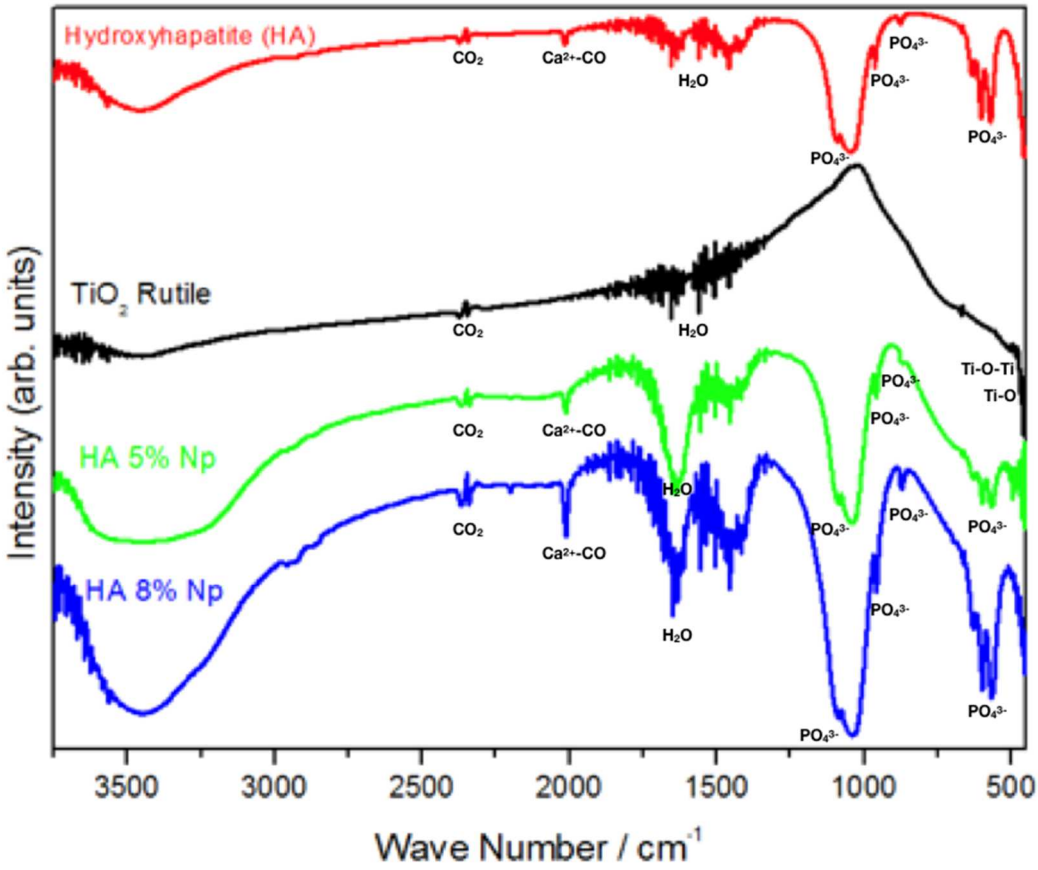


*Figure 3. FTIR spectra of starting ceramic powder.*

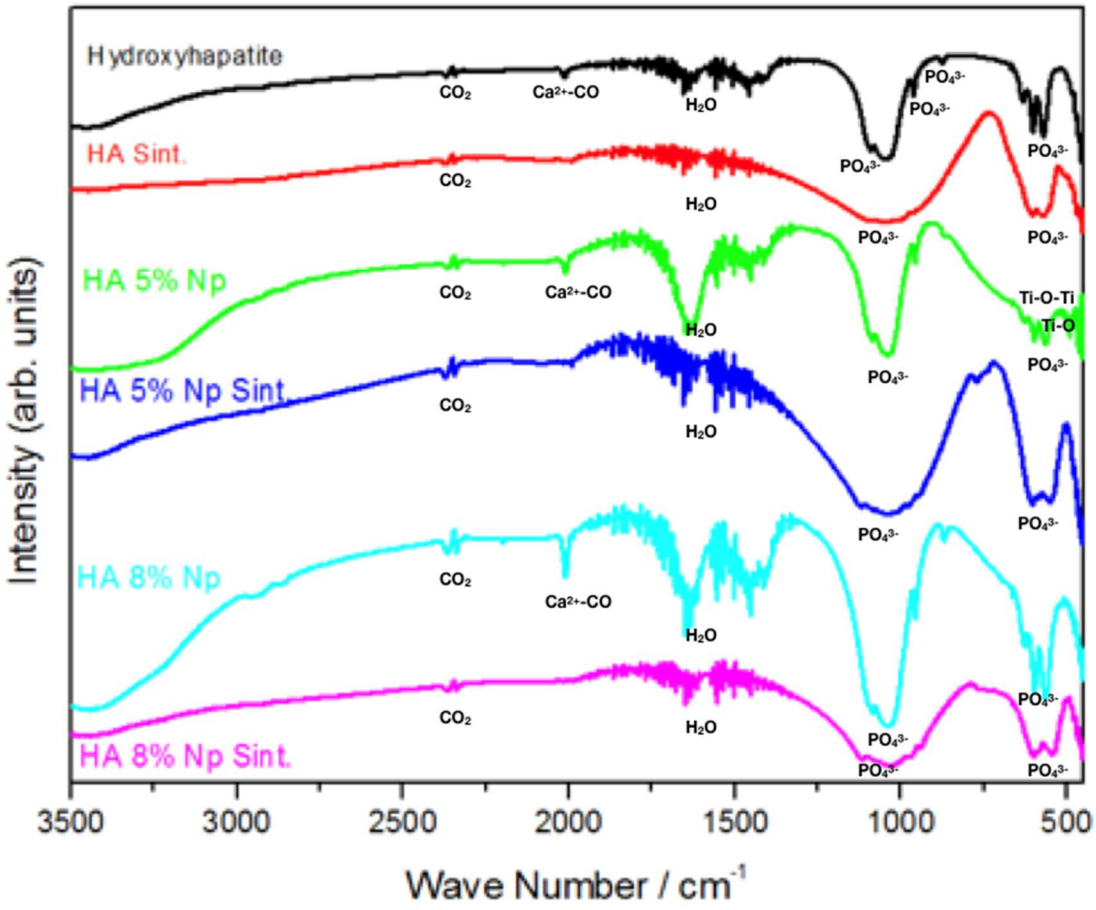


*Figure 4. FTIR spectra of powder and sintered ceramic specimens.*

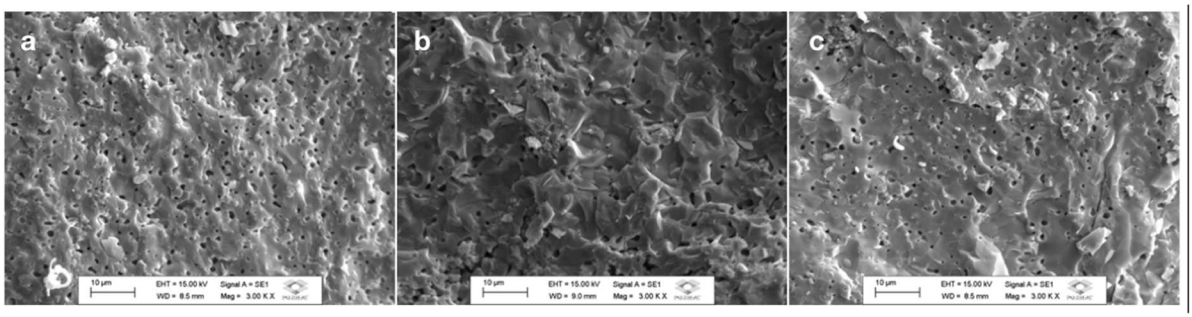


*Figure 5. FE-SEM of groups (a) Pure Ha, (b) HA/5%$TiO_2$np and (c) HA/8%$TiO_2$np*

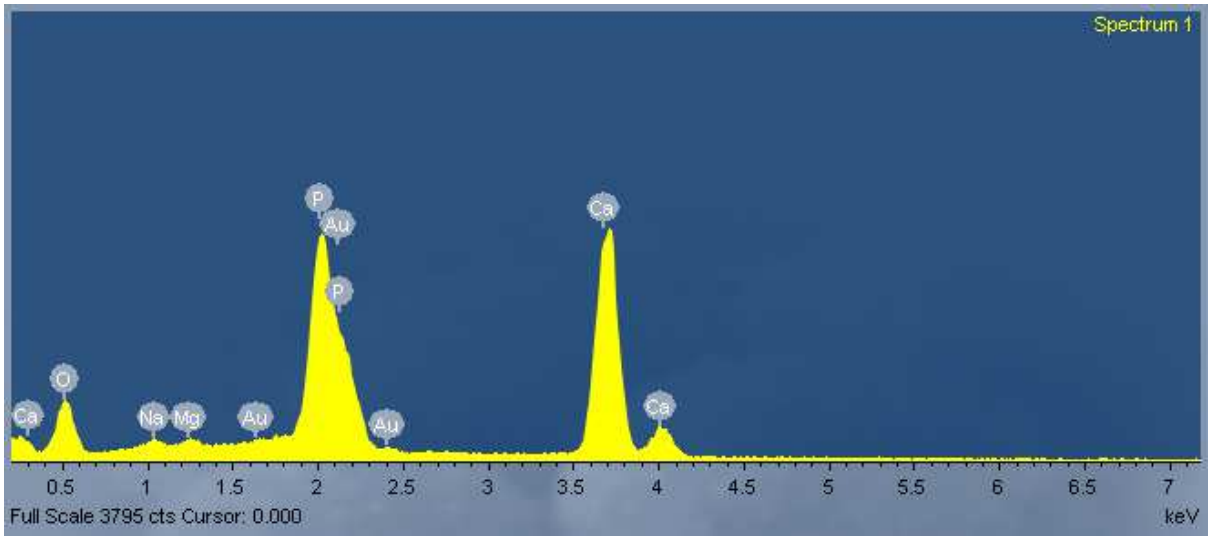


*Figure 6. EDS analysis of Pure HA specimen external surface. Note the predominance of P, Ca, followed by O, Mg and Na.*

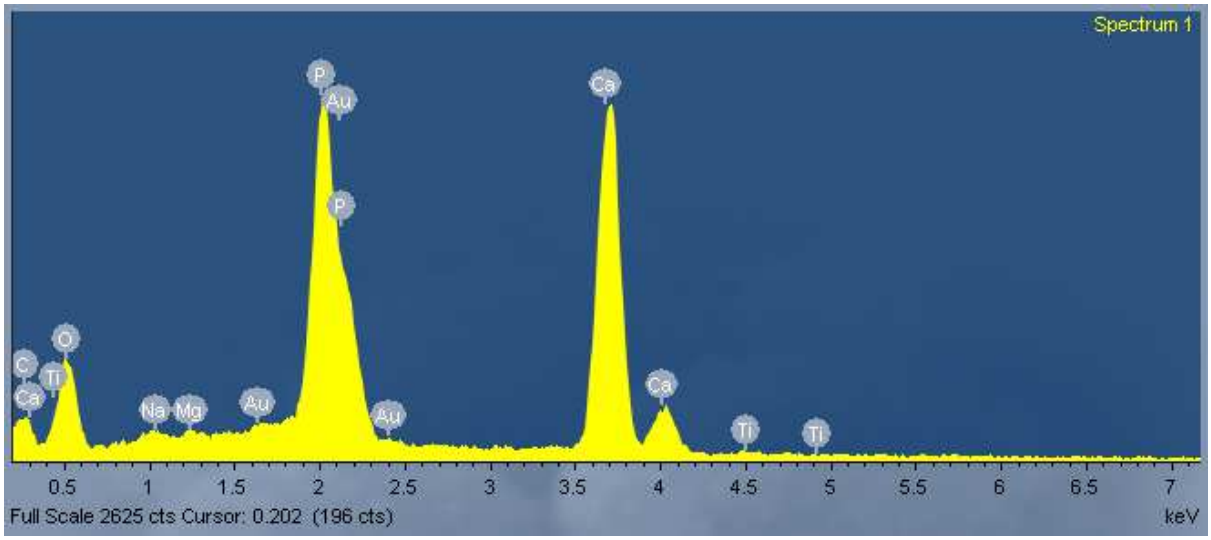


*Figure 7. EDS analysis of HA5%npTiO$_2$ specimen external surface. Note the predominance of P, Ca, followed by Ti, C, O, Mg, and Na.*

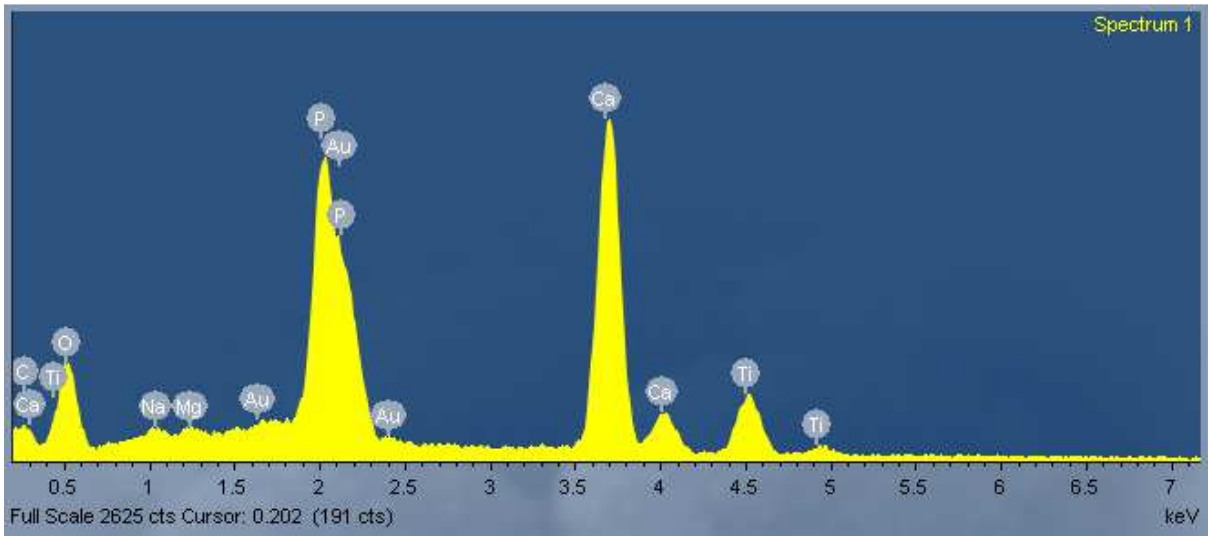


*Figure 8. EDS analysis of HA8%npTiO$_2$ specimen external surface. Note the predominance of P, Ca, followed by Ti, C, O, Mg, Na.*

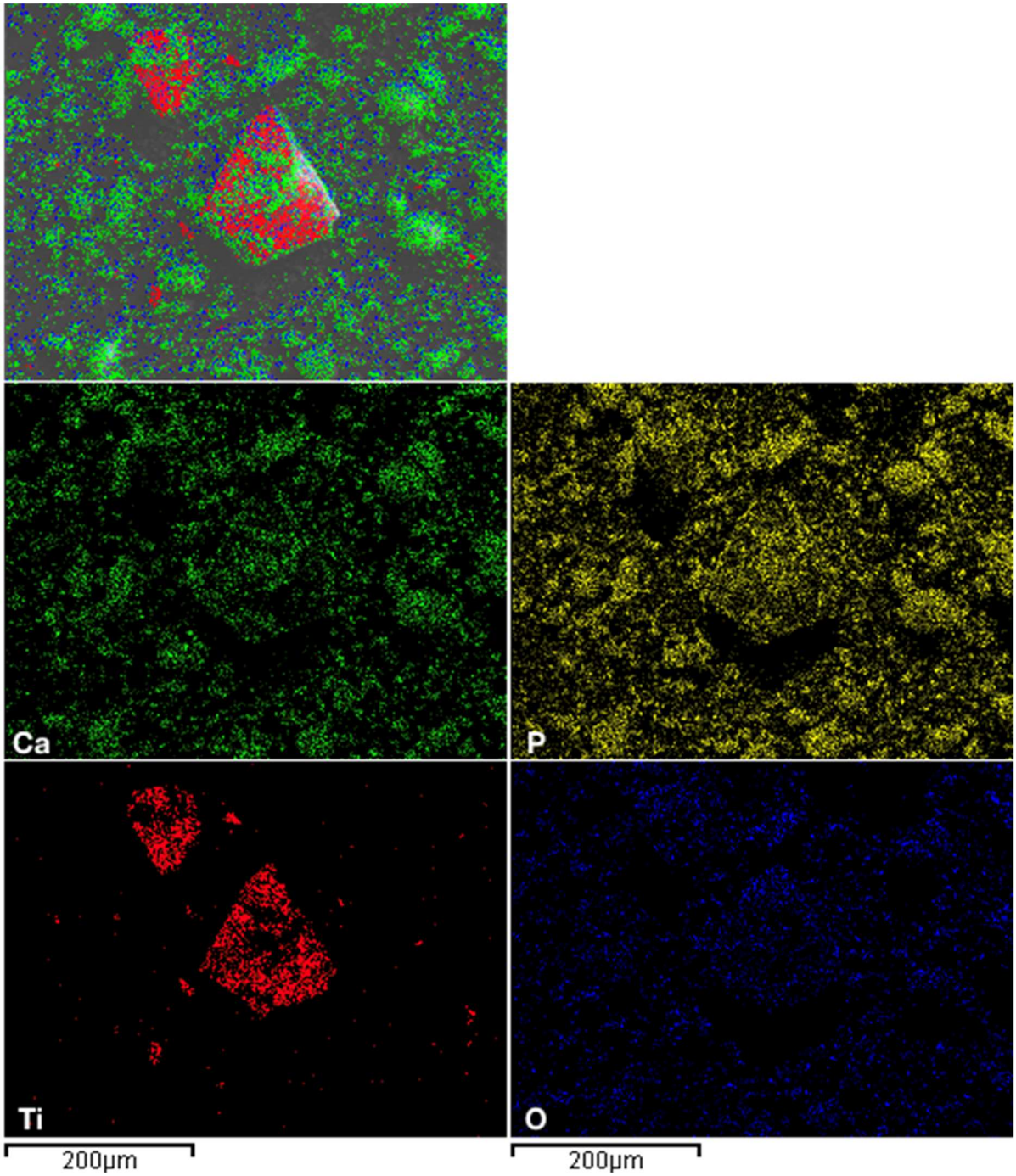


*Figure 9. EDS mapping of HA5%np$TiO_2$ group. Note that Ti was red-identified in a non-homogeneous spreading, different from the Ca, P and O spreading patterns.*

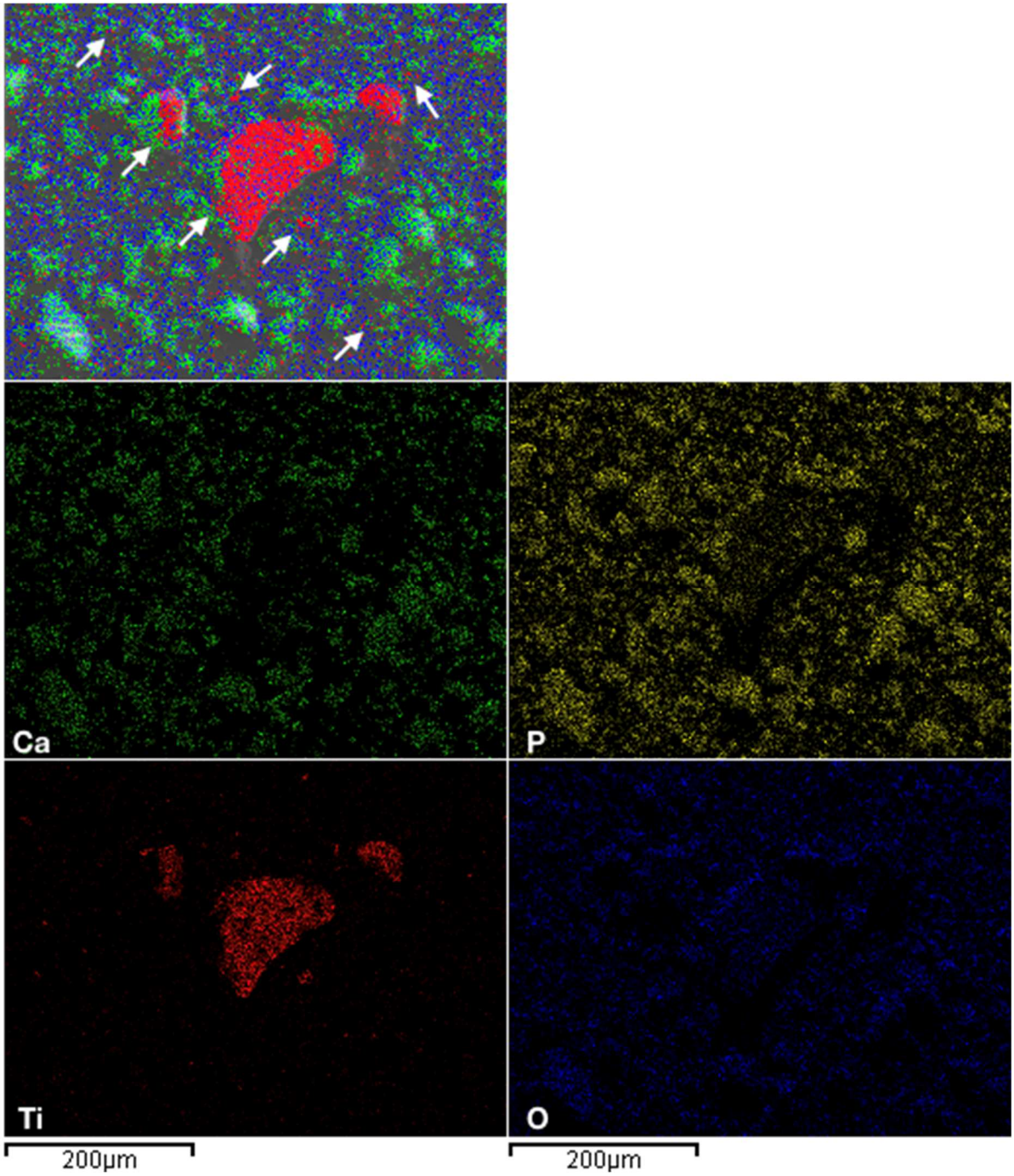


*Figure 10. EDS mapping of HA8%np$TiO_2$ group. Note that Ti was red-identified in a more homogeneous spreading compared to the HA5%np$TiO_2$ group (white arrows)*